frontiers in Chemistry

ORIGINAL RESEARCH
published: 08 September 2021
doi: 10.3389/fchem.2021.736285

Preparation of Sepiolite Nanofibers Supported Zero Valent Iron Composite Material for Catalytic Removal of Tetracycline in Aqueous Solution

Xiaoyu Han[1,2], *Hong Zhang*[1,2], *Caihong Zhang*[1,2], *Yan Zhao*[1,2], *Na Zhang*[1,2] *and Jinsheng Liang*[1,2]*

[1]*Key Laboratory of Special Functional Materials for Ecological Environment and Information (Hebei University of Technology), Ministry of Education, Tianjin, China,* [2]*Institute of Power Source and Ecomaterials Science, Hebei University of Technology, Tianjin, China*

The heavy use of antibiotics in medicine, stock farming and agriculture production has led to their gradual accumulation in environmental media, which poses a serious threat to ecological environment and human safety. As an efficient and promising catalyst for the degradation of antibiotics, nanoscale zero valent iron (nZVI) has attracted increasing attention in recent years. In this study, sepiolite nanofiber supported zero valent iron (nZVI/SEP) composite was prepared via a facile and environmentally friendly method. The nZVI particles (with size of 20–60 nm) were dispersed evenly on the surface of sepiolite nanofibers, and the catalytic performance for the removal of tetracycline hydrochloride (TC-HCl) in aqueous system was investigated. The effect of nZVI loading amount, catalyst dosage, H_2O_2 concentration and pH on the removal efficiency of TC-HCl were studied. It was revealed that the sepiolite supporter effectively inhibited the agglomeration of nZVI particles and increased the contact area between contaminant and the active sites, resulting in the higher catalytic performance than pure nZVI material. The TC-HCl removal efficiency of nZVI/SEP composite was up to 92.67% when TC-HCl concentration of 20 mg/L, catalyst dosage of 1.0 g/L, H_2O_2 concentration of 1.0 mM, pH value of 7. Therefore, the nZVI/SEP composites possess high catalytic activity for TC-HCl removal and have great application prospects in antibiotic wastewater treatment.

Keywords: sepiolite, nanoscale zero valent iron, green synthesis, catalytic performance, antibiotic degradation

OPEN ACCESS

Edited by:
Yunfei Xi,
Queensland University of Technology, Australia

Reviewed by:
Wenbo Wang,
Inner Mongolia University, China
Priyabrat Mohapatra,
C. V. Raman College of Engineering, India

****Correspondence:***
Jinsheng Liang
liang_jinsheng@sina.com

Specialty section:
This article was submitted to Green and Sustainable Chemistry, a section of the journal Frontiers in Chemistry

Received: *05 July 2021*
Accepted: *25 August 2021*
Published: *08 September 2021*

Citation:
Han X, Zhang H, Zhang C, Zhao Y, Zhang N and Liang J (2021) Preparation of Sepiolite Nanofibers Supported Zero Valent Iron Composite Material for Catalytic Removal of Tetracycline in Aqueous Solution. Front. Chem. 9:736285. doi: 10.3389/fchem.2021.736285

INTRODUCTION

In recent years, refractory organic pollutants such as antibiotics (Ouyang et al., 2019; Chen et al., 2020a), mycotoxins (Li et al., 2018; Sun et al., 2020) and drugs (Daneshkhah et al., 2017; Phasuphan et al., 2019) have become emerging environmental issues because of the rapid development of pharmaceutical industry, agriculture and animal husbandry. Particularly, the abuse of antibiotics has led to the gradual accumulation in soil and water environments, which enhances the bacterial resistance and endangers various ecosystems (Dong et al., 2018; Pirsaheb et al., 2019). Among various antibiotics, tetracycline is the most extensively used antibiotic around the world because of its low cost and high antimicrobial activities (Xu et al., 2020; Zhao et al., 2020). However, only a small fraction of tetracycline can be metabolized or adsorbed by humans or animals, 50–80% residuals and

metabolites enter into the environment. Thus, tetracycline antibiotics with low biodegradability have been frequently detected in soil and water (Hou et al., 2020; Zhang et al., 2021). Tetracycline accumulation in the environment readily leads to cause bacterial resistance to antibiotics, which poses a serious threat to human health and ecological security. Consequently, the removal of antibiotics has been paid close attention by the scientific researchers in the fields of biology, chemistry, medicine and environment. General technologies, such as biodegradation, absorption, coagulation and sedimentation, have a limited impact on the removal of various antibiotics. In comparison, the advanced oxidation processes (AOPs) can generate highly reactive free radicals to efficiently degrade antibiotics (Huang et al., 2020).

Nanoscale zero-valent iron (nZVI) has been proved as an effective material for the removal of organic and inorganic contaminants because of its high reactivity and low toxicity of reaction products (Hemmat et al., 2021). In Fenton-like process, nZVI can be acted as a source of Fe^{2+}. The produced Fe^{2+} reacts with hydrogen peroxide (H_2O_2) to form OH, which has strong oxidizing ability to efficiently degrades and mineralize organic contaminants in aquatic system (Pirsaheb et al., 2019; Zhou et al., 2019). However, nZVI materials exhibit certain deficiencies in practical applications including strong tendency to aggregation and oxidation, secondary iron pollution, difficult separation and recovery (Bossa et al., 2017; Nasiri et al., 2019; Gopal et al., 2020). Particularly, the aggregation of nZVI particles will significantly affect the mobility and effective surface area to reduce the catalytic activities. To overcome these problems, it has been proposed to load nZVI particles on various supports like clay minerals (Frost et al., 2010; Bao et al., 2019), zeolite (Suazo-Hernandez et al., 2019), silica materials (Guo et al., 2021), activated carbon (Huang et al., 2019) and biochar (Zhang et al., 2020).

Sepiolite is a natural hydrated magnesium silicate mineral with chemical formula of $Mg_8Si_{12}O_{30}(OH)_4(OH_2)_4$ $8H_2O$. And it is a 2:1 phyllosilicate composed of two Si-O tetrahedral layers and an intermediate layer of Mg-O(OH) octahedral (Rao et al., 2018). The sepiolite with abundant micropores and channels possesses high surface area and strong absorbability, which should be in favor of conducting contaminants to the reactive cites of the composite materials resulting in the improvement of degradation efficiency (Ezzatahmadi et al., 2017). Daneshkhah et al. (2017) synthesized sepiolite-supported nanoscale zerovalent iron by sodium borohydride reduction method to removal metoprolol from water. Habish et al. (2017) studied the composites with different radio of sepiolite and nanoscale zerovalent iron to achieve the best nZVI dispersibility and the highest adsorption capacity for Cd^{2+}. However, there are few studies on the utilization of nZVI-sepiolite composites for the removal of antibiotic contaminants.

Because no toxic reducing agents (like $NaBH_4$) or nitrogen protection and other harsh processing conditions are needed, green synthesis is more suitable for large-scale production of nZVI materials (Badmus et al., 2018; Mondal et al., 2020). Martins et al. (2017) compared the environmental impacts and costs between sodium borohydride reduction (traditional synthesis) and green synthesis method by life cycle assessment (LCA). The results showed that the green synthesis presented 50% lower environmental impacts than the sodium borohydride reduction, and the traditional synthesis was much more expensive than the green synthesis (roughly eight times higher). In this study, the sepiolite nanofiber supported nZVI composites (nZVI/SEP) were synthesized by green method. In the course of green synthesis, the biologically-active substances from plant extracts (green tea, coffee, eucalyptus leaves, grape leaves, pomegranate leaves, etc.) can both reduce the Fe^{2+} or Fe^{3+} and effectively prevent nanoparticles from oxidation. Among them, green tea extracts are kinds of excellent reducing and capping agents owing to the large amounts of polyphenols substances. The prepared nZVI/SEP composites were employed as Fenton-like catalyst to remove tetracycline hydrochloride (TC-HCl) from aqueous solutions. The surface morphology and micropore structure of the nZVI/SEP composite were characterized. And the effects of reaction time, TC-HCl initial concentration, catalyst dosage, H_2O_2 concentration, and pH on TC-HCl degradation process were investigated.

MATERIALS AND METHODS

Materials

The natural sepiolite used in the experiments was obtained from Nanyang of Henan Province. Its chemical composition (wt%) was: SiO_2, 39.20; MgO, 17.00; CaO, 32.40; Al_2O_3, 6.20; Fe_2O_3, 3.46, MnO, 0.40; TiO_2, 0.27; K_2O, 0.21 and Na_2O, 0.20. The natural sepiolite was firstly treated with 2 mol/L HCl solution in a magnetic stirrer for stirring 12 h at room temperature for impurity removal and activation. The solid was filtered and centrifuged, washed several times with deionized water, and then dried at 80°C for 10 h. All chemical regents used in this work, tetracycline hydrochloride ($C_{22}H_{24}N_2O_8$ HCl, 98% purity), H_2O_2 (30 wt %), HCl (37 wt%), and $FeCl_3$ $6H_2O$ were of analytical grade and used without further purification.

Preparation of nZVI/SEP Composite

To prepare green tea extract, dried green tea (15 g) was added to 250 ml deionized water in round bottom flask. The mixture was then heated up to boiling at 80°C for 1 h and then filtering the extract to remove tea leaves. The green tea extracts were stored at 4°C until further use.

For the synthesis of nZVI/SEP composite, a certain amount of sepiolite was added to the conical flask and mixed with 0.1 M $FeCl_3$ solution (the SEP:nZVI mass ratio was 10:1, 8:1, 5:1, 2:1, respectively), and the equal volume of green tea extract was dropped into the flask while continuously stirring at room temperature and the solution immediately turned black. The black particles were collected by centrifuging followed by washing several times with deionized water and absolute ethanol. Finally, the obtained particles were dried under vacuum at 60°C for 12 h. The obtained composites were denoted as 0.1 nZVI/SEP, 0.125nZVI/SEP, 0.2nZVI/SEP, 0.5 nZVI/SEP, respectively.

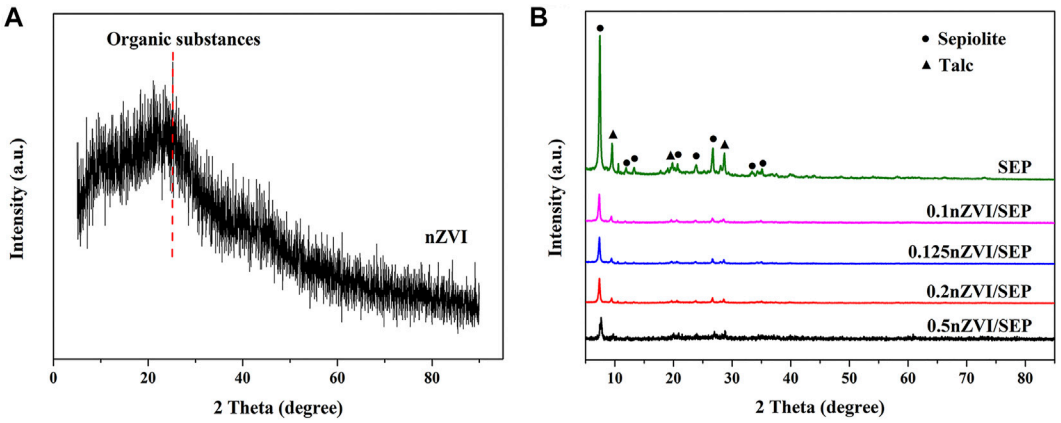

FIGURE 1 | XRD patterns of **(A)** nZVI, **(B)** SEP and nZVI/SEP composites.

Characterization of nZVI/SEP Composite

The X-ray diffraction (XRD) patterns were performed using a Bruker D8 Advance diffractometer with Cu Kα radiation over 2θ ranging from 10° to 90°. The morphologies and structures of the samples were observed by scanning electron microscopy (SEM, FEI Nano SEM450) and transmission electron microscopy (TEM, Philips Tecnai G2 F20). The X-ray photoelectron spectroscopy (XPS, Thermo Fisher ESCALAB 250Xi) was used to determine the elemental composition of sample surface. Fourier transform infrared spectroscopy (FTIR) spectra were recorded using a Bruker V80 spectrometer in the range of 4,000–400 cm^{-1}. Nitrogen adsorption desorption isotherms were measured at −196°C using a Quantach rome Autosorb iQ2 analyzer. The specifc surface area of the samples was calculated according to the Brunauer-Emmett-Teller (BET) method, and the pore volumes were taken at P/P0 = 0.990 single point. The pore size distributions were calculated by the Barrett-Joyner-Halenda (BJH) method.

Batch Experiments

TC-HCl was chosen as the target pollutant to evaluate the catalytic performance of nZVI/SEP. For each experiment, 100 ml of TC-HCl solution with a certain concentration (10, 20, 30, 50 and 80 mg/L) was added to the conical flasks at room temperature. After that, certain dosages of catalyst (0.5, 1.0, and 1.5 g/L) and H_2O_2 (0.5, 1.0 and 1.5 mM) were added to the solution. The solution pH (4, 5 and 6) was adjusted by 0.1 M HCl and 0.1 M NaOH solution. After the obtained mixture was shaken for a predetermined time (30, 60, 90, 120, 180 and 240 min), the supernatant solution was separated from the catalyst by centrifugation at 5,000 rpm for 5 min. Then the concentration of TC-HCl supernatant was measured by UV–vis spectrophotometer at the 357 nm wavelength. The removal efficiency (R) of TC-HCl was calculated as follows:

$$R(\%) = \frac{C_0 - C_t}{C_0} \times 100\% \quad (1)$$

where C_0 (mg/L) is the initial concentration and C_t (mg/L) is the concentration of TC-HCl at reaction time t (min).

RESULTS AND DISCUSSION

Characterization of nZVI/SEP Composite

Figure 1 shows the XRD pattern of the sepiolite, synthesized nZVI and nZVI/SEP composite. The XRD pattern shows the characteristic peak of sepiolite at 2θ = 7.3°, which is consistent with the reference material. A little amount of talc impurity is also observed in the SEP sample. There is no sharp diffraction peak observed in the pattern of nZVI, indicating that the synthesized nZVI is essentially amorphous. And the broad shoulder peak at around 2θ = 22.6° can be identified as amorphous carbon, which suggests that organic molecules from the green tea extract have successfully combined with nZVI and coated the surface of the nZVI particles. Besides, typical Fe^0 diffraction peaks cannot be observed in the patterns of nZVI/SEP composites. It is probably because the low loading amount and absence of crystallinity of iron. Similar results are reported in literatures (Liu et al., 2018; Yazdani et al., 2019; Lin et al., 2020).

The surface morphologies of SEP, nZVI and nZVI/SEP composite are presented in **Figure 2**. The SEM images reveal that the sepiolite particles exhibit a characteristic fibrous morphology, and the nZVI particles shows obviously aggregated spherical particles, with sizes between 100 and 200 nm. As for the nZVI/SEP composite, the surface of sepiolite observed with conspicuous granule, demonstrating that the nZVI particles are uniformly distributed throughout the sepiolite fibers without aggregation. And the size of nZVI particles in nZVI/SEP composites is less than 100 nm, which are significant decreased compared with the pure nZVI. The elemental mapping image of nZVI/SEP further reveals the homogeneous immobilization of nZVI particles on nZVI/SEP composite surface. From the distribution of elements Fe and C, it can be concluded that the oxidized polyphenols from green tea act as stabilizing and capping agent coated on the surface of nZVI particles.

The particle shape and size of nZVI, dispersity of nZVI/SEP composite are further investigated by TEM. From **Figure 3A**, the nZVI particles are approximately spherical in shape with the

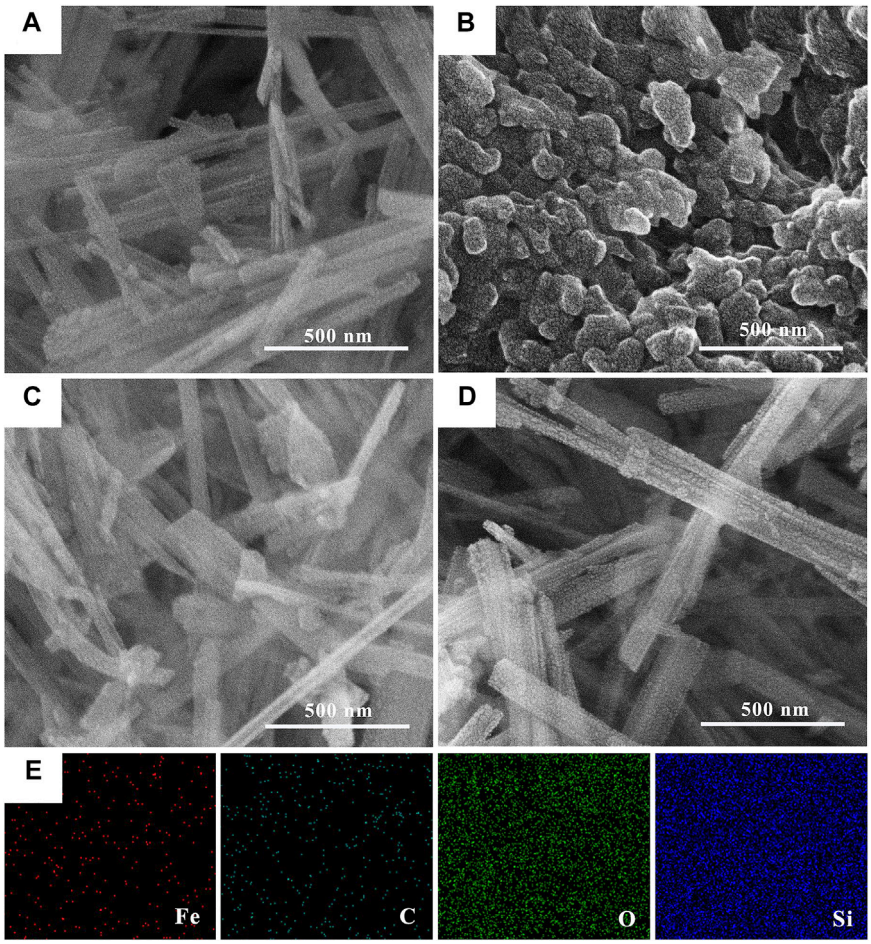

FIGURE 2 | SEM images of **(A)** SEP, **(B)** nZVI, **(C, D)** nZVI/SEP composites and **(E)** the element mapping of nZVI/SEP composites.

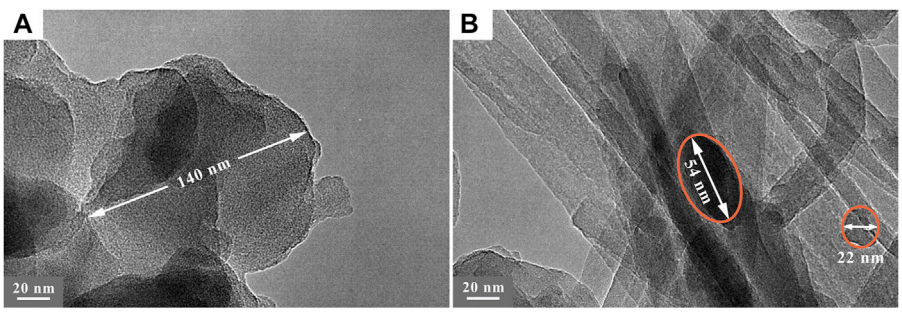

FIGURE 3 | TEM images of **(A)** nZVI and **(B)** nZVI/SEP composite.

diameter around 140 nm, and the Fe^0 grains are encapsulate by a layer of membranous substance. The membranous substance is considered to amorphous carbon derived from green tea extract, which is consistent with the results of element mapping. Although polyphenols in green tea as stabilizing agent can reduce electrostatic repulsion and steric hindrance, some aggregation still can be observed in nZVI sample because of the magnetic interaction of nZVI particles. In **Figure 3B**, the nZVI particles are well dispersed and attached to sepiolite fibers as individual spherical shaped particles, and the particle size is much smaller than the pure nZVI particles. It indicates that sepiolite fiber supported nZVI described in this work is an

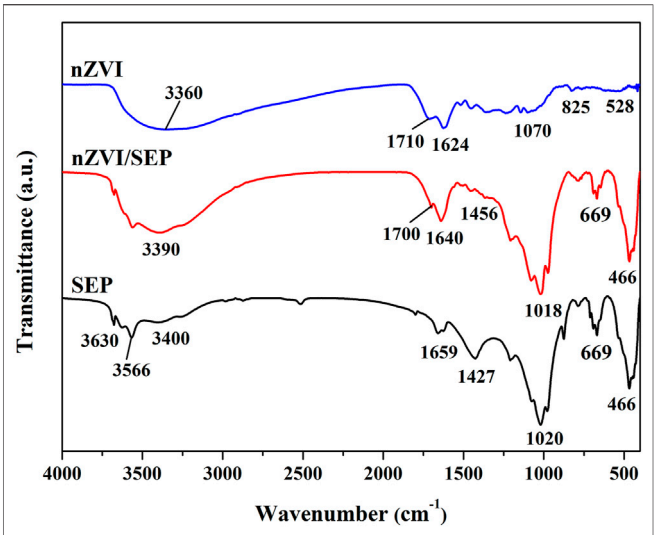

FIGURE 4 | FTIR spectra of SEP, nZVI and nZVI/SEP samples.

effective approach to improve the dispersion properties and applied performances of Fe^0 nanoparticles.

The FTIR spectra of SEP, nZVI and nZVI/SEP are carried out in the range of 400–4,000 cm^{-1} and the results are shown in **Figure 4**. The peaks in the region around 3,400–3,600 cm^{-1} corresponds to O-H stretching vibration owing to the water molecule and hydroxyl-band (Mg_3OH) of SEP, whereas the peaks at 1,659 and 669 cm^{-1} correspond to O-H bending vibration (Daneshkhah et al., 2017; Wu et al., 2017). The peak at 1,020 cm^{-1} is assigned to the Si-O stretching vibration of sepiolite tetrahedral sheets. And the peak at 466 cm^{-1} is assigned to the Si-O-Si bending vibration (Thao et al., 2018). The peak at 1,427 cm-1 relates to the C-O stretching vibration of carbonate impurity (Ma et al., 2017). For nZVI sample, the broad peak around 3,360 cm^{-1} is attributed to the O-H stretching vibration of polyphenols from green tea extract in synthesis of Fe nanoparticles. The peak at 1710 cm^{-1} is assigned to C=O stretching vibration of carbonyl groups derived from polyphenols. Moreover, the peak at 1,624 cm^{-1} can be ascribed

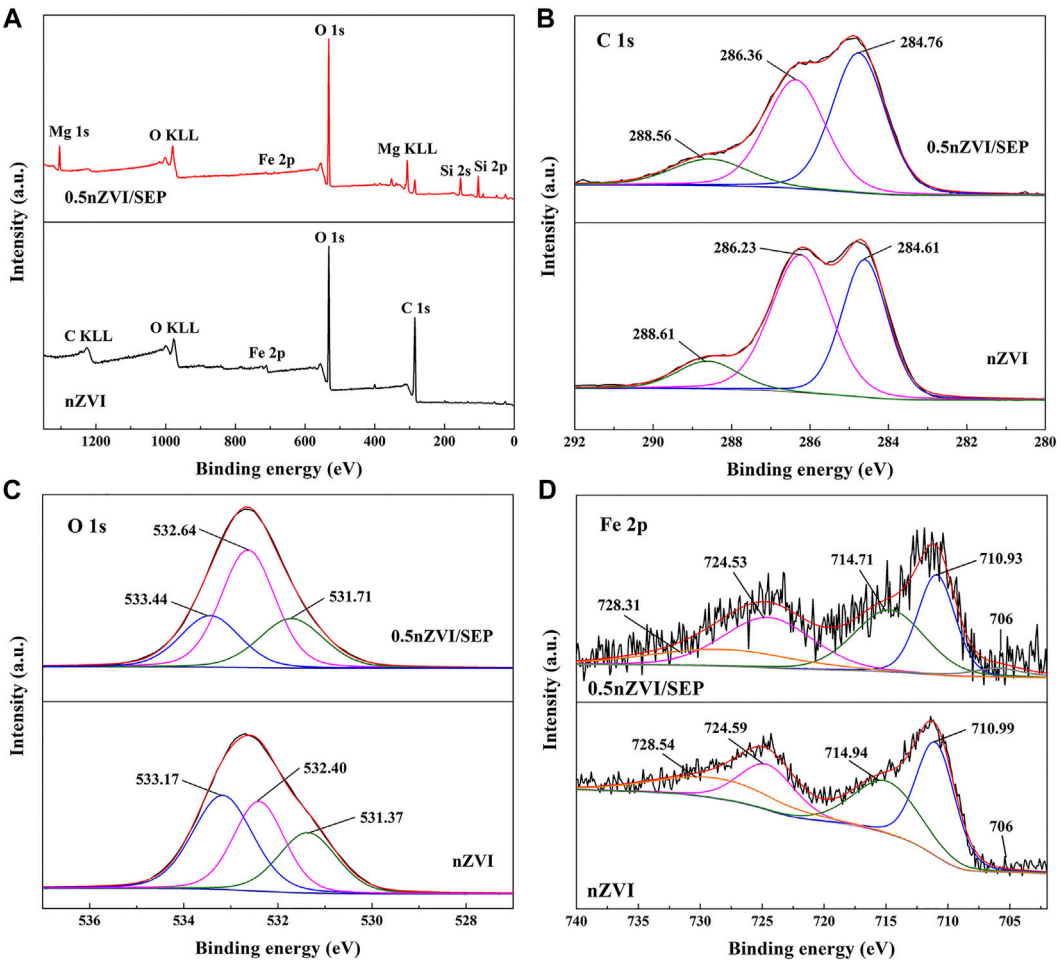

FIGURE 5 | XPS spectra of **(A)** full-range scan spectra of nZVI and nZVI/SEP, and **(B)** Fe 2p, **(C)** C 1s and **(D)** O 1s of nZVI/SEP composite.

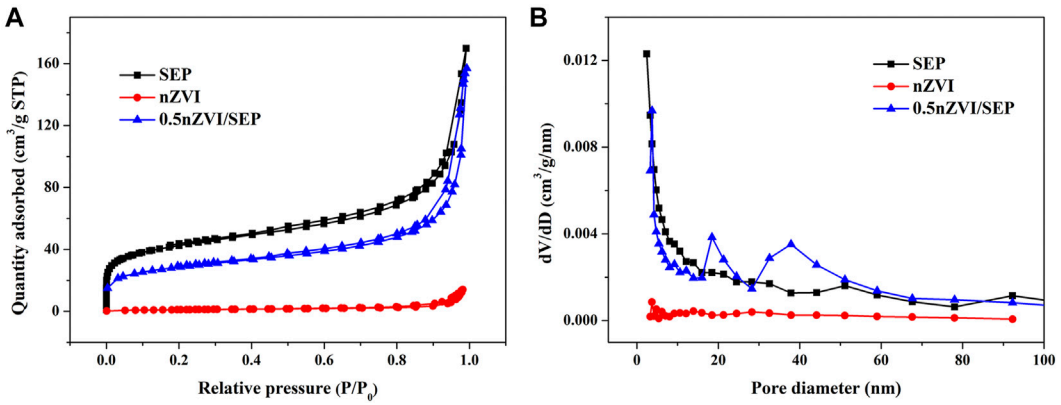

FIGURE 6 | (A) N_2 adsorption-desorption isotherms and **(B)** pore size distribution of SEP, nZVI and nZVI/SEP composite.

to the C=C stretching vibration of aromatic ring (Wang et al., 2017), while the peak at 1,070 cm^{-1} is ascribed to C-O-C stretching vibration (Liu et al., 2017). In addition, the weak absorption band at 825 and 528 cm^{-1} is attributed to Fe-O stretching vibration of Fe oxide (Wang et al., 2020), which confirm properly the synthesis of nZVI particles. After nZVI loaded on the surface of sepiolite, it is observed that several peaks are disappeared or shifted because of the interaction of the functional groups existing on SEP and nZVI. These changes prove the successful loading and immobilization of nZVI particles on sepiolite fibers.

XPS is performed to investigate the composition and chemical states of nZVI and nZVI/SEP as shown in **Figure 5**. From the full scan spectra (**Figure 5A**), it can be clearly observed that synthesized nZVI is composed of Fe, C and O, while nZVI/SEP composite is composed of Fe, Si, Mg, O and C. The result indicates that Fe^0 is successfully synthesized *via* green method and loaded on the surface of sepiolite. **Figure 5B** presents the C 1s spectra, and the binding energy of 284.61, 286.23, and 288.61 eV are contributed to C-C, C-O and C=O, respectively (Balachandramohan and Sivasankar, 2018). As shown in **Figure 5C**, the O 1s spectra at 533.17 eV indicates the oxygen bonding to carbon. The peak at 531.71 eV is assigned to the lattice oxygen (O^{2-}) of metal oxide, and the peak at 532.40 eV is owing to the hydroxyl groups (-OH) (Liu et al., 2018). Consequently, the spectra of C 1s and O 1s confirm that some biomolecules (mainly amorphous carbon) from green tea extract are capped on the surface of nZVI particles, the result is consistent with TEM analysis. For the Fe 2p high-resolution spectrum of nZVI (**Figure 5D**), two peaks at 710.99 eV (Fe $2P_{3/2}$) and 724.59 eV (Fe $2p_{1/2}$) are assigned to Fe_2O_3. And the binding energy at 714.94 eV (Fe $2P_{3/2}$) and 728.54 qeV (Fe $2p_{1/2}$) are attributed to octahedrally-coordinated Fe^{3+} from hydroxides (FeOOH) (Chen et al., 2020a). Moreover, the weak peaks around 706 eV in nZVI and 0.5nZVI/SEP are also observed, which correspond to the Fe $2P_{3/2}$ for Fe^0. Because of the high reactivity of nZVI particles, the Fe^0 is easily oxidized in the process of preparation and storage, thus forming a layer of iron oxides on the surface of Fe^0. The presence of surface substances (amorphous carbon and iron oxides) of nZVI particles limit the Fe^0 detection, since XPS is a sensitive surface analysis technique with only 2–5 nm detection depth (Ma et al., 2016; Nguyen et al., 2019).

TABLE 1 | Pore structural characteristics of SEP, nZVI and nZVI/SEP composites.

Sample	S_{BET} (m^2/g)	V (cm^3/g)	D_{BJH} (nm)
SEP	152.78	0.2581	6.7566
nZVI	4.04	0.0216	21.3890
0.1n ZVI/SEP	122.90	0.2456	7.9919
0.125 nZVI/SEP	115.36	0.2397	8.2650
0.2 nZVI/SEP	104.55	0.2341	8.7187
0.5 nZVI/SEP	101.35	0.2285	9.0194

Catalytic activity of heterogeneous catalysts is closely related to their pore structure, which supply active sites for contaminants. Thus, N_2 adsorption-desorption analyses of SEP, nZVI and nZVI/SEP composite were carried out, and the isotherms as well as the pore size distribution are shown in **Figure 6**. According to the IUPAC classification, the isotherms of all three samples belong to the typical type IV and H3 hysteresis loops, indicating the presence of mesoporous structure. However, the adsorption amount of pure nZVI is well below than SEP and nZVI/SEP composite, this is probably because nZVI particles are tend to agglomerate, resulting in the lower specific surface area. And the pore size distribution diagram indicates that the pore diameter of these samples is mainly distributed between 3 and 50 nm, which further proves that the nZVI/SEP composite have abundant mesopores and wide pore size distribution.

Table 1 shows the BET surface area, total pore volume and average pore size of SEP, nZVI and nZVI/SEP composites. The BET results reveal that the specific surface area of nZVI/SEP composite decreases with the increase of loading amount of nZVI, which may be attributed to the partial blocking of the pores by nZVI loaded on sepiolite surface. Besides, the pore size of nZVI/SEP composites increases gradually due to the formation of larger mesopores accumulated by nZVI on sepiolite fibers. Compare with the pure nZVI, the nZVI/SEP composites exhibit higher specific surface area and larger number of mesopores, which confirming that nZVI particles are well dispersed on sepiolite

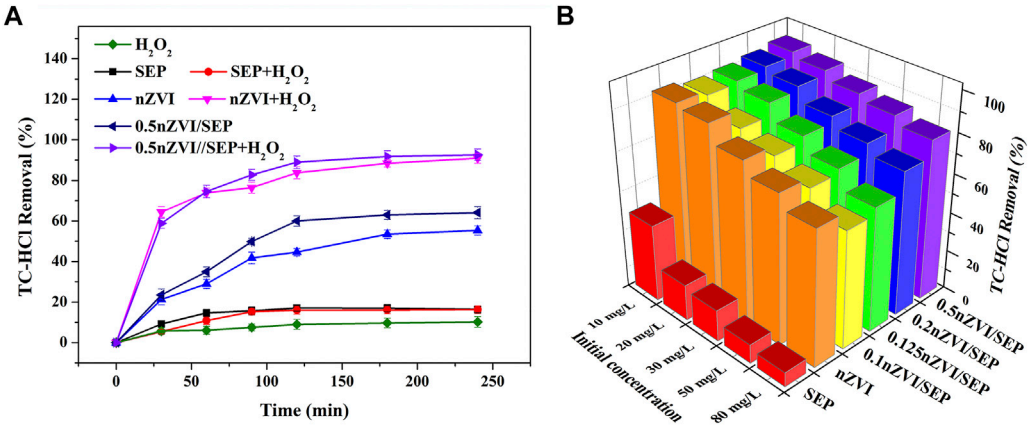

FIGURE 7 | (A) TC-HCl removal in different systems, **(B)** TC-HCl removal efficiency by different catalysts. (Experimental conditions: TC-HCl concentration = 20 mg/L, catalyst dosage = 0.1 g/L, H_2O_2 concentration = 1 mM, pH = 7, room temperature).

surface without significant aggregation. Therefore, porous structure of nZVI/SEP composites provide a large number of reaction sites for better contract between the catalyst and pollutants.

TC-HCl Removal by Synthesized Catalyst

Tetracycline hydrochloride is amphoteric compound with multiple ionizable functional groups. When pH is below 3.30, TC-HCl primary exists in the form of cation, zwitterion as main form when pH value is between 3.30 and 7.68, while forming the anion when pH is above 7.68 (Yang et al., 2018; Sun et al., 2021). In this study, the removal efficiency of TC-HCl was investigated under various systems, catalyst dosage, H_2O_2 concentration and pH value.

The effect of different systems on the removal of TC-HCl are shown in **Figure 7A**. There is no obvious removal efficiency for TC-HCl of H_2O_2, suggesting that H_2O_2 alone is unable to degrade TC-HCl because of its poor oxidation ability. And SEP shows poor TC-HCl adsorption, only 16.48% of TC-HCl is removed within 240 min. Instead, nZVI and nZVI/SEP composite show good degradation effect for TC-HCl, the final removal efficiency of 240 min is about 55.37 and 64.15%, respectively. Furthermore, TC-HCl removal efficiency is dramatically improved after adding H_2O_2 into the nZVI and nZVI/SEP system, and the removal efficiency can be up to 90.93 and 92.67%, respectively. Considering the minor role of TC-HCl adsorption, TC-HCl removal is mainly attributed to heterogeneous catalysis, and the presence of zero valent iron is favorable to the Fenton-like reaction. **Figure 7B** shows the removal efficiency of different catalysts for TC-HCl with different initial concentration of TC-HCl. It is seen that sepiolite support zero valent iron exhibits excellent catalytic performance compared with pure nZVI and SEP. And the TC-HCl removal efficiency of the nZVI/SEP composites significantly improve with the increasing of nZVI loading amounts. When the loading amount of nZVI is 0.2, the removal efficiency of nZVI/SEP composite for TC-HCl with different concentration is higher than pure nZVI. 0.5 nZVI/SEP shows the best degradation effect for different concentrations of TC-HCl. The removal efficiencies of 10 mg/L, 20 mg/L, 30 mg/L, 50 mg/L and 80 mg/L TC-HCl are reach 95.36, 92.67, 88.26, 85.08 and 80.97% respectively. Although the adsorption of TC-HCl on sepiolite is negligible under the condition of different concentrations of TC-HCl, the large specific surface area of sepiolite enhances the initial contact between nZVI particles and TC-HCl, as well as improves the dispersion of nZVI particles, thus increasing the number of active sites as a result.

The relationship between reaction time and removal efficiency of TC-HCl by different nZVI/SEP composites are described in **Figure 8A**. For four nZVI/SEP composites, the TC-HCl removal curves look similar, and their reaction rates are faster within 60 min and then the removal efficiency gradually increase with the increase of reaction time. The TC-HCl removal efficiency on these samples all can reach over 80% in about 180 min. The catalyst with high loading amount of nZVI have higher degradation efficiency of TC-HCl. However, when the loading amount of nZVI is more than 50%, the removal efficiency for TC-HCl of nZVI/SEP composite may decrease attributed to the aggregation of nZVI at higher content. Therefore, the catalyst of 0.5 nZVI/SEP is selected to study the effects of catalyst dosage, H_2O_2 concentration and pH on TC-HCl removal.

The effect of catalyst dosages on TC-HCl removal efficiency is shown in **Figure 8B**. It can be observed that the TC-HCl removal efficiency increases from 87.62 to 94.77% with the catalyst dosage increasing from 0.5 to 1.5 g/L. It can be explained that the catalytic activity is closely related to the quantity of active sites, higher dosage of catalyst lead to more Fe^{2+} ions generated from nZVI (**Eq. 2**). Subsequently, Fe^{2+} combines with H_2O_2 to create more hydroxyl radicals (**Eq. 3**) which possess high oxidizing ability toward TC-HCl.

$$Fe^0 + H_2O_2 + 2H^+ \rightarrow Fe^{2+} + 2H_2O \quad (2)$$

$$Fe^{2+} + H_2O_2 \rightarrow Fe^{3+} + \cdot OH + OH^- \quad (3)$$

In the heterogeneous Fenton system, hydroxyl radical is mainly produced from H_2O_2, which has a direct influence on

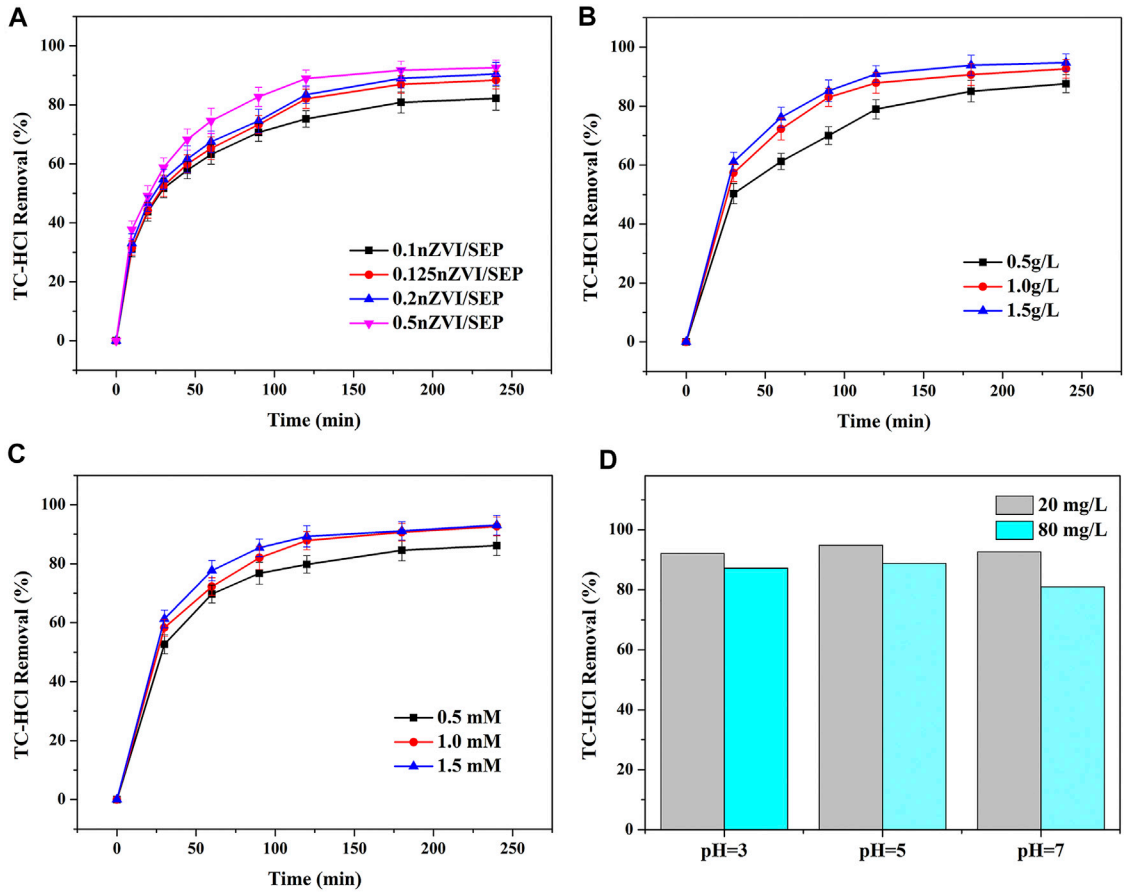

FIGURE 8 | Effect of **(A)** loading amount of nZVI, **(B)** catalyst dosage, **(C)** H_2O_2 concentration, **(D)** pH value on TC-HCl removal by 0.5 nZVI/SEP. (Experimental conditions: TC-HCl concentration = 20 mg/L, catalyst dosage = 0.1 g/L, H_2O_2 concentration = 1 mM, pH = 7, room temperature).

the degradation of TC-HCl (Qin et al., 2020; Wu et al., 2020). From **Figure 8C**, the TC-HCl removal efficiency increases from 86.15 to 92.67% with increasing H_2O_2 concentration from 0.5 to 1.0 mM. When the concentration of H_2O_2 is low, the degradation of TC-HCl is not complete, which may be due to the lack of enough OH in aqueous solution. With the H_2O_2 concentration increasing, the amount of OH in the system also increases, which accelerates the degradation of TC-HCl and improves the removal efficiency of TC-HCl. However, a slight improvement in TC-HCl removal efficiency is observed as the H_2O_2 concentration continues rising to 1.5 mM. It is because a limited number of active sites only react with a certain number of H_2O_2 molecules, and excessive H_2O_2 could not decompose to produce more hydroxyl radicals. Moreover, excessive H_2O_2 has been proved to promote the reaction of OH with H_2O_2 and HO_2, resulting in the scavenging effect of OH (**Equations 4**, **5**).

$$H_2O_2 + \cdot OH \rightarrow H_2O + \cdot HO_2 \quad (4)$$

$$\cdot HO_2 + \cdot OH \rightarrow H_2O + O_2 \quad (5)$$

The pH value is a significant factor in the TC-HCl degradation process. And the removal of TC-HCl by oxidation shows better performance in acidic condition than neutral and alkaline condition. It is probably because the surface of nZVI particles is prone to corrosion under acidic condition (Cao et al., 2018; Cao et al., 2019; Nie et al., 2020), and leading to a large number of Fe^{2+} release (**Eq. 6**). The increased Fe^{2+} reacts with H_2O_2 to generate more hydroxyl radicals, which promotes the oxidation of TC-HCl *via* Fenton-like reaction. As the increase of pH value, nZVI tended to form a passive oxide layer to block the reaction sites, and hence decreasing the degradation effect (Dong et al., 2018). In addition, H_2O_2 is easily decomposed into oxygen and water at alkaline conditions. As shown in **Figure 8D**, initial pH 5 has the highest TC-HCl removal efficiency. At pH = 5, the removal efficiency of 20 mg/L TC-HCl is 94.79% while 80 mg/L TC-HCl is 88.79%. However, when the pH value is too low, it will promote the release of hydrogen (**Eq. 7**), which produces air bubbles on the surface of catalyst. Moreover, nZVI can be able to dissolve rapidly in strong acidic condition, which limits the Fenton-like oxidation process as well as the production of H_2O_2 (Chen et al., 2020a).

$$Fe^0 + O_2 + 2H^+ \rightarrow H_2O_2 + Fe^{2+} \quad (6)$$

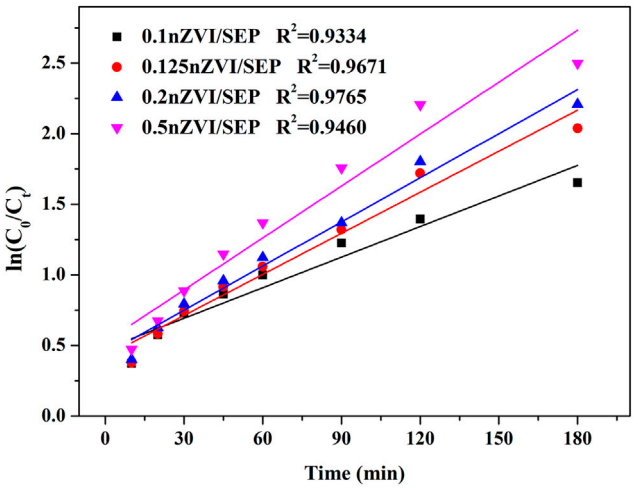

FIGURE 9 | Pseudo-first-order kinetic curve of TC-HCl degradation. (Experimental conditions: TC-HCl concentration = 20 mg/L, catalyst dosage = 0.1 g/L, H_2O_2 concentration = 1 mM, pH = 7, room temperature).

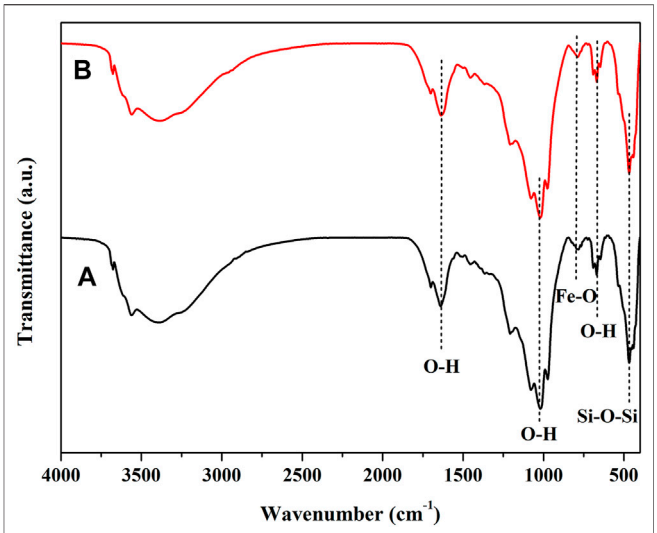

FIGURE 10 | FTIR spectra of 0.5nZVI/SEP sample **(A)** before and **(B)** after the reaction with TC-HCl.

$$Fe^0 + 2H^+ \rightarrow Fe^{2+} + H_2 \quad (7)$$

Kinetic Study

Generally, the pseudo-first-order kinetic model is extensively used to describe the Fenton-like process (Wang et al., 2021). The model can be expressed as follows:

$$ln\frac{C_0}{C_t} = kt \quad (8)$$

Where C_0 is the initial concentration (mg/L), C_t is the concentration of TC-HCl at reaction time t (mg/L), k is the apparent rate constant (min^{-1}), and t is the reaction time (min).

Figure 9 shows the pseudo-first-order fitting curves of 0.1nZVI/SEP, 0.125 nZVI/SEP, 0.2 nZVI/SEP and 0.5 nZVI/SEP samples, and the corresponding reaction rate constant is 0.00722, 0.00969, 0.01042 and 0.01226 min^{-1}, respectively. It reflects that the nZVI/SEP + H_2O_2 system is highly effective for TC-HCl degradation. And the reaction rate constant of TC-HCl degradation process is consistent with the previous reports (Zhang et al., 2018; Khodadadi et al., 2019; Xin et al., 2021). The 0.5nZVI/SEP composite exhibits highest catalytic efficiency, which indicates that the loading amount of nZVI is closely related to the catalytic performance of TC-HCl.

Comparison of Tetracycline Removal Efficiency With Various Catalysts

The tetracycline removal efficiency of nZVI/SEP composite prepared in this work is compared to other related catalysts reported in literature and the result is listed in **Table 2**. It is clear that the nZVI/SEP composite displays excellent catalytic performance for tetracycline antibiotic under different conditions. Moreover, raw materials like green tea and sepiolite used in this work are cheap, easily available, safe and non-toxic. The synthesis process of nZVI/SEP composite is also simple and can be used in large-scale production. Hence, the synthesized nZVI/SEP composite can be employed as a suitable catalyst for the degradation of antibiotics in aqueous solution.

TABLE 2 | Comparison of removal efficiency of various catalysts for tetracycline.

Catalyst	Catalyst dosage (g/L)	H_2O_2	TC (mg/L)	pH	Removal efficiency (%)	Reference
nZVI/SEP	1.0	1 mM	20	7	92.67	This work
Fe-MOFs	0.2	44 mM	10	5.0	83.3	Geng et al. (2021)
Fe^0/CeO^2	0.1	100 mM	100	5.8	91	Zhang et al. (2019)
Fe-biochar	1	5 mM	40	7.4	90.7	Bao et al. (2021)
Fe-loaded granular activated carbon	3.0	10 ml/L	10	2	87.01	Pan et al. (2019)
Fe-Mn binary oxide	0.4	1% wt	30	5	95	Chen et al. (2020b)
Mesoporous bimetallic Fe/Co	0.6	0.25 mol/L	30	7.0	86	Li et al. (2019)
Fe_3O_4 nanospheres	0.5	50 mM	25	7	82	Nie et al. (2020)
Fe-Co oxide nanosheet	0.3	20 mM	50	7	83.57	Nie et al. (2021)
Fe loaded graphitic carbon	0.02	1.0 mM	40	4.3	83	Wang et al. (2021)

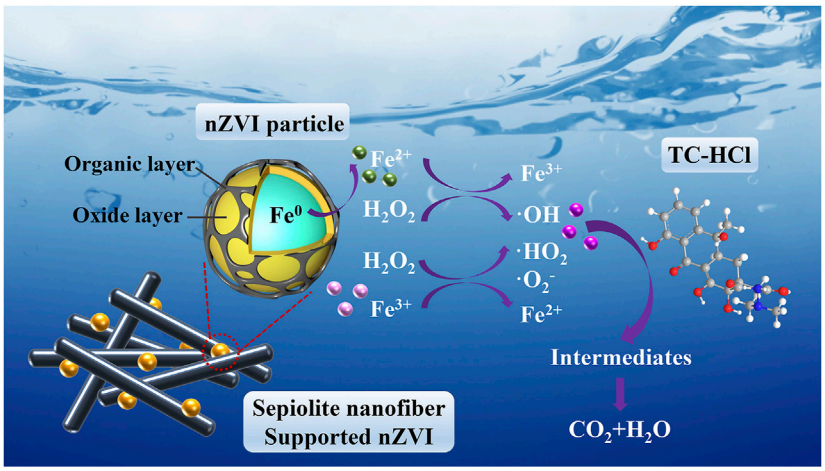

FIGURE 11 | Removal mechanism for TC-HCl on nZVI/SEP composite in Fenton-like system.

Passible Degradation Mechanism of TC-HCl by nZVI/SEP Composite

To investigate the interactions between the nZVI/SEP catalyst and TC-HCl, FTIR spectra of 0.5nZVI/SEP before and after the reaction were compared. As shown in **Figure 10**, there are no obvious characteristic peaks of TC-HCl in the spectrum after the reaction, which suggests that few TC-HCl is adsorbed to the catalytic surface. Consequently, only the degradation process in the reaction is discussed below.

Based on the experimental results and discussions above, a passible degradation mechanism for TC-HCl removal by nZVI/SEP composite in Fenton-like system is proposed and the diagrammatic sketch is depicted in **Figure 11**. The introduction of sepiolite can result in a better catalytic performance. On the one hand, sepiolite effectively inhibits the agglomeration of nZVI particles and reduces the size of nZVI particles, which can enhance the mobility and dispersion of nZVI particles and promote the direct contact between nZVI particles and contaminants in aqueous solution. On the other hand, the sepiolite supported nZVI composites possess the large specific surface area and porous structure, which is beneficial to conduct the contaminants to the reactive cites of the catalyst and then accelerating the degradation rate. Therefore, the NZVI/SEP composite is more efficient catalyst relative to either pure nZVI or sepiolite in removing TC-HCl antibiotic. In addition, there is a layer of capping agent (mainly amorphous carbon) on the surface of NZVI particles synthesized by green method, which can prevent the faster oxidation of Fe^0 in practical application, and slow down the dissolution of NZVI particles because of the protection of surface capping. It leads to the slow release of active species to realize excellent degradation performance for antibiotic contaminants (Monga et al., 2020).

In the heterogeneous Fenton-like process, ·OH radical is the main ROS and plays a predominant role in TC-HCl degradation (Pan et al., 2019; Wang et al., 2021). Firstly, the addition of H_2O_2 accelerates the corrosion of Fe0, resulting in plenty of Fe^{2+} continuously produced (**Eq. 2**). Then the Fe^{2+} reacts with H_2O_2 and generates sufficient OH radicals (**Eq. 3**). And Fe^{3+} can be reduced to Fe^{2+} with the presence of Fe0 in the Fenton reaction (**Eq. 9**. In addition, the redox cycle of Fe^{2+}/Fe^{3+} also promotes the generation of $HO_2/\cdot O_2^-$ radicals (**Eqs 10**, **11**). During this process, because of the high specific surface area and nanofiber structure of sepiolite, it is beneficial to promote the direct contact between TC-HCl and catalyst, as well as provide more reaction sites for H_2O_2 activation. Finally, OH radicals on the surface of catalyst can efficiently degrade TC-HCl and the TC-HCl is degraded into some intermediates by OH and $HO_2/\cdot O_2^-$ radicals and eventually mineralized into CO_2 and H_2O (Luo et al., 2020).

$$2Fe^{3+} + Fe^0 \rightarrow 3Fe^{2+} \quad (9)$$

$$Fe^{3+} + H_2O_2 \rightarrow Fe^{2+} + \cdot HO_2 + H^+ \quad (10)$$

$$Fe^{3+} + \cdot HO_2 \rightarrow Fe^{2+} + O_2 + H^+ \quad (11)$$

CONCLUSIONS

The zero valent iron particles were successfully loaded via green method onto sepiolite nanofiber at different nZVI/SEP ratios. It was observed that the spherical nZVI particles are well dispersed on the surface of sepiolite nanofibers with particle size of 20–60 nm. Moreover, the nZVI/SEP composite show larger specific surface area (101.35 m^2/g) than pure nZVI (4.04 m^2/g). Synthesized nZVI/SEP composites were applied for the degradation of TC-HCl antibiotic from aqueous solution. The nZVI/SEP composites exhibited higher removal efficiency of TC-HCl, which because the sepiolite inhibited the agglomeration of nZVI particles and improved the mobility and dispersion. Furthermore, sepiolite as support promoted the change of contact between high reactive sites and TC-HCl contaminant, thereby significantly increasing the catalytic activity. In order to explore the degradation mechanism of TC-HCl by nZVI/SEP composite. The effects of initial TC-HCl concentration, catalyst dosage, H_2O_2 concentration

and pH value were also investigated. The efficient removal of TC-HCl was achieved in the catalyst/H_2O_2 system due to the combination of Fe0 reduction and Fenton oxidation processes. This work suggests that nZVI/SEP composite has great potential for remediation of antibiotic wastewater.

DATA AVAILABILITY STATEMENT

The original contributions presented in the study are included in the article/Supplementary Material, further inquiries can be directed to the corresponding author.

AUTHOR CONTRIBUTIONS

XH and JL developed the concept and designed the experiment; XH and CZ conducted the experiments. YZ and NZ helped analysis the data. XH wrote the first draft of the manuscript; HZ and JL revised the manuscript.

FUNDING

This work was supported by the Innovation Teams and Leading Talents Plan (Hebei, China).

REFERENCES

Badmus, K. O., Coetsee-Hugo, E., Swart, H., and Petrik, L. (2018). Synthesis and Characterisation of Stable and Efficient Nano Zero Valent Iron. *Environ. Sci. Pollut. Res.* 25, 23667–23684. doi:10.1007/s11356-018-2119-7

Balachandramohan, J., and Sivasankar, T. (2018). Ultrasound Assisted Synthesis of Guar Gum-Zero Valent Iron Nanocomposites as a Novel Catalyst for the Treatment of Pollutants. *Carbohydr. Polym.* 199, 41–50. doi:10.1016/j.carbpol.2018.06.097

Bao, D., Li, Z., Tang, R., Wan, C., Zhang, C., Tan, X., et al. (2021). Metal-modified Sludge-Based Biochar Enhance Catalytic Capacity: Characteristics and Mechanism. *J. Environ. Manage.* 284, 112113. doi:10.1016/j.jenvman.2021.112113

Bao, T., Jin, J., Damtie, M. M., Wu, K., Yu, Z. M., Wang, L., et al. (2019). Green Synthesis and Application of Nanoscale Zero-Valent Iron/rectorite Composite Material for P-Chlorophenol Degradation via Heterogeneous Fenton Reaction. *J. Saudi Chem. Soc.* 23, 864–878. doi:10.1016/j.jscs.2019.02.001

Bossa, N., Carpenter, A. W., Kumar, N., de Lannoy, C.-F., and Wiesner, M. (2017). Cellulose Nanocrystal Zero-Valent Iron Nanocomposites for Groundwater Remediation. *Environ. Sci. Nano* 4, 1294–1303. doi:10.1039/c6en00572a

Cao, J., Lai, L., Lai, B., Yao, G., Chen, X., and Song, L. (2019). Degradation of Tetracycline by Peroxymonosulfate Activated with Zero-Valent Iron: Performance, Intermediates, Toxicity and Mechanism. *Chem. Eng. J.* 364, 45–56. doi:10.1016/j.cej.2019.01.113

Cao, J., Xiong, Z., and Lai, B. (2018). Effect of Initial pH on the Tetracycline (TC) Removal by Zero-Valent Iron: Adsorption, Oxidation and Reduction. *Chem. Eng. J.* 343, 492–499. doi:10.1016/j.cej.2018.03.036

Chen, L., Ni, R., Yuan, T., Gao, Y., Kong, W., Zhang, P., et al. (2020a). Effects of green Synthesis, Magnetization, and Regeneration on Ciprofloxacin Removal by Bimetallic nZVI/Cu Composites and Insights of Degradation Mechanism. *J. Hazard. Mater.* 382, 121008. doi:10.1016/j.jhazmat.2019.121008

Chen, Y., Zeng, Z., Li, Y., Liu, Y., Chen, Y., Wu, Y., et al. (2020b). Glucose Enhanced the Oxidation Performance of Iron-Manganese Binary Oxides: Structure and Mechanism of Removing Tetracycline. *J. Colloid Interf. Sci.* 573, 287–298. doi:10.1016/j.jcis.2020.04.006

Daneshkhah, M., Hossaini, H., and Malakootian, M. (2017). Removal of Metoprolol from Water by Sepiolite-Supported Nanoscale Zero-Valent Iron. *J. Environ. Chem. Eng.* 5, 3490–3499. doi:10.1016/j.jece.2017.06.040

Dong, H., Jiang, Z., Zhang, C., Deng, J., Hou, K., Cheng, Y., et al. (2018). Removal of Tetracycline by Fe/Ni Bimetallic Nanoparticles in Aqueous Solution. *J. Colloid Interf. Sci.* 513, 117–125. doi:10.1016/j.jcis.2017.11.021

Ezzatahmadi, N., Ayoko, G. A., Millar, G. J., Speight, R., Yan, C., Li, J., et al. (2017). Clay-supported Nanoscale Zero-Valent Iron Composite Materials for the Remediation of Contaminated Aqueous Solutions: A Review. *Chem. Eng. J.* 312, 336–350. doi:10.1016/j.cej.2016.11.154

Frost, R. L., Xi, Y., and He, H. (2010). Synthesis, Characterization of Palygorskite Supported Zero-Valent Iron and its Application for Methylene Blue Adsorption. *J. Colloid Interf. Sci.* 341, 153–161. doi:10.1016/j.jcis.2009.09.027

Geng, N., Chen, W., Xu, H., Ding, M., Lin, T., Wu, Q., et al. (2021). Insights into the Novel Application of Fe-MOFs in Ultrasound-Assisted Heterogeneous Fenton System: Efficiency, Kinetics and Mechanism. *Ultrason. Sonochem.* 72, 105411. doi:10.1016/j.ultsonch.2020.105411

Gopal, G., Kvg, R., M, S., J, L. A. A., Chandrasekaran, N., and Mukherjee, A. (2020). Green Synthesized Fe/Pd and *In-Situ* Bentonite-Fe/Pd Composite for Efficient Tetracycline Removal. *J. Environ. Chem. Eng.* 8, 104126. doi:10.1016/j.jece.2020.104126

Guo, Y., Chen, B., Zhao, Y., and Yang, T. (2021). Fabrication of the Magnetic Mesoporous Silica Fe-MCM-41-A as Efficient Adsorbent: Performance, Kinetics and Mechanism. *Sci. Rep.* 11, 2612. doi:10.1038/s41598-021-81928-8

Habish, A. J., Lazarević, S., Janković-Častvan, I., Jokić, B., Kovač, J., Rogan, J., et al. (2017). Nanoscale Zerovalent Iron (nZVI) Supported by Natural and Acid-Activated Sepiolites: the Effect of the nZVI/support Ratio on the Composite Properties and Cd2+ Adsorption. *Environ. Sci. Pollut. Res.* 24, 628–643. doi:10.1007/s11356-016-7802-y

Hemmat, K., Khodabakhshi, M. R., and Zeraatkar Moghaddam, A. (2021). Synthesis of Nanoscale Zero-valent Iron Modified Graphene Oxide Nanosheets and its Application for Removing Tetracycline Antibiotic: Response Surface Methodology. *Appl. Organomet. Chem.* 35, e6059. doi:10.1002/aoc.6059

Hou, X., Shi, J., Wang, N., Wen, Z., Sun, M., Qu, J., et al. (2020). Removal of Antibiotic Tetracycline by Metal-Organic Framework MIL-101(Cr) Loaded Nano Zero-Valent Iron. *J. Mol. Liquids* 313, 113512. doi:10.1016/j.molliq.2020.113512

Huang, T., Liu, L., Zhang, S., and Xu, J. (2019). Evaluation of Electrokinetics Coupled with a Reactive Barrier of Activated Carbon Loaded with a Nanoscale Zero-Valent Iron for Selenite Removal from Contaminated Soils. *J. Hazard. Mater.* 368, 104–114. doi:10.1016/j.jhazmat.2019.01.036

Huang, X., Zhu, N., Wei, X., Ding, Y., Ke, Y., Wu, P., et al. (2020). Mechanism Insight into Efficient Peroxydisulfate Activation by Novel Nano Zero-Valent Iron Anchored yCo3O4 (nZVI/yCo3O4) Composites. *J. Hazard. Mater.* 400, 123157. doi:10.1016/j.jhazmat.2020.123157

Khodadadi, M., Hossein Panahi, A., Al-Musawi, T. J., Ehrampoush, M. H., and Mahvi, A. H. (2019). The Catalytic Activity of FeNi3@SiO2 Magnetic Nanoparticles for the Degradation of Tetracycline in the Heterogeneous Fenton-like Treatment Method. *J. Water Process Eng.* 32, 100943. doi:10.1016/j.jwpe.2019.100943

Li, J., Li, X., Han, J., Meng, F., Jiang, J., Li, J., et al. (2019). Mesoporous Bimetallic Fe/o as Highly Active Heterogeneous Fenton Catalyst for the Degradation of Tetracycline Hydrochlorides. *Sci. Rep.* 9, 15820. doi:10.1038/s41598-019-52013-y

Li, Y., Tian, G., Dong, G., Bai, S., Han, X., Liang, J., et al. (2018). Research Progress on the Raw and Modified Montmorillonites as Adsorbents for Mycotoxins: A Review. *Appl. Clay Sci.* 163, 299–311. doi:10.1016/j.clay.2018.07.032

Lin, Z., Weng, X., Owens, G., and Chen, Z. (2020). Simultaneous Removal of Pb(II) and Rifampicin from Wastewater by Iron Nanoparticles Synthesized by a tea Extract. *J. Clean. Prod.* 242, 118476. doi:10.1016/j.jclepro.2019.118476

Liu, J., Mwamulima, T., Wang, Y., Fang, Y., Song, S., and Peng, C. (2017). Removal of Pb(II) and Cr(VI) from Aqueous Solutions Using the Fly Ash-Based Adsorbent Material-Supported Zero-Valent Iron. *J. Mol. Liquids* 243, 205–211. doi:10.1016/j.molliq.2017.08.004

Liu, Y., Jin, X., and Chen, Z. (2018). The Formation of Iron Nanoparticles by Eucalyptus Leaf Extract and Used to Remove Cr(VI). *Sci. Total Environ.* 627, 470–479. doi:10.1016/j.scitotenv.2018.01.241

Luo, T., Feng, H., Tang, L., Lu, Y., Tang, W., Chen, S., et al. (2020). Efficient Degradation of Tetracycline by Heterogeneous Electro-Fenton Process Using Cu-Doped Fe@Fe2O3: Mechanism and Degradation Pathway. *Chem. Eng. J.* 382, 122970. doi:10.1016/j.cej.2019.122970

Ma, L., Rathnayake, S. I., He, H., Zhu, R., Zhu, J., Ayoko, G. A., et al. (2016). *In Situ* sequentially Generation of Acid and Ferrous Ions for Environmental Remediation. *Chem. Eng. J.* 302, 223–232. doi:10.1016/j.cej.2016.05.065

Ma, Y., Wu, X., and Zhang, G. (2017). Core-shell Ag@Pt Nanoparticles Supported on Sepiolite Nanofibers for the Catalytic Reduction of Nitrophenols in Water: Enhanced Catalytic Performance and DFT Study. *Appl. Catal. B: Environ.* 205, 262–270. doi:10.1016/j.apcatb.2016.12.025

Martins, F., Machado, S., Albergaria, T., and Delerue-Matos, C. (2017). LCA Applied to Nano Scale Zero Valent Iron Synthesis. *Int. J. Life Cycle Assess.* 22, 707–714. doi:10.1007/s11367-016-1258-7

Mondal, P., Anweshan, A., and Purkait, M. K. (2020). Green Synthesis and Environmental Application of Iron-Based Nanomaterials and Nanocomposite: A Review. *Chemosphere* 259, 127509. doi:10.1016/j.chemosphere.2020.127509

Monga, Y., Kumar, P., Sharma, R. K., Filip, J., Varma, R. S., Zbořil, R., et al. (2020). Sustainable Synthesis of Nanoscale Zerovalent Iron Particles for Environmental Remediation. *ChemSusChem* 13, 3288–3305. doi:10.1002/cssc.202000290

Nasiri, J., Motamedi, E., Naghavi, M. R., and Ghafoori, M. (2019). Removal of crystal Violet from Water Using β-cyclodextrin Functionalized Biogenic Zero-Valent Iron Nanoadsorbents Synthesized via Aqueous Root Extracts of Ferula Persica. *J. Hazard. Mater.* 367, 325–338. doi:10.1016/j.jhazmat.2018.12.079

Nguyen, M. T., Yu, K., Tokunaga, T., Boonyaperm, K., Kheawhom, S., Arita, M., et al. (2019). Green Synthesis of Size-Tunable Iron Oxides and Iron Nanoparticles in a Salt Matrix. *ACS Sust. Chem. Eng.* 7, 17697–17705. doi:10.1021/acssuschemeng.9b03950

Nie, M., Li, Y., He, J., Xie, C., Wu, Z., Sun, B., et al. (2020). Degradation of Tetracycline in Water Using Fe3O4 Nanospheres as Fenton-like Catalysts: Kinetics, Mechanisms and Pathways. *New J. Chem.* 44, 2847–2857. doi:10.1039/d0nj00125b

Nie, M., Li, Y., Li, L., He, J., Hong, P., Zhang, K., et al. (2021). Ultrathin Iron-Cobalt Oxide Nanosheets with Enhanced H2O2 Activation Performance for Efficient Degradation of Tetracycline. *Appl. Surf. Sci.* 535, 147655. doi:10.1016/j.apsusc.2020.147655

Ouyang, Q., Kou, F., Zhang, N., Lian, J., Tu, G., and Fang, Z. (2019). Tea Polyphenols Promote Fenton-like Reaction: pH Self-Driving Chelation and Reduction Mechanism. *Chem. Eng. J.* 366, 514–522. doi:10.1016/j.cej.2019.02.078

Pan, L., Cao, Y., Zang, J., Huang, Q., Wang, L., Zhang, Y., et al. (2019). Preparation of Iron-Loaded Granular Activated Carbon Catalyst and its Application in Tetracycline Antibiotic Removal from Aqueous Solution. *Ijerph* 16, 2270. doi:10.3390/ijerph16132270

Phasuphan, W., Praphairaksit, N., and Imyim, A. (2019). Removal of Ibuprofen, Diclofenac, and Naproxen from Water Using Chitosan-Modified Waste Tire Crumb Rubber. *J. Mol. Liquids* 294, 111554. doi:10.1016/j.molliq.2019.111554

Pirsaheb, M., Moradi, S., Shahlaei, M., Wang, X., and Farhadian, N. (2019). A New Composite of Nano Zero-Valent Iron Encapsulated in Carbon Dots for Oxidative Removal of Bio-Refractory Antibiotics from Water. *J. Clean. Prod.* 209, 1523–1532. doi:10.1016/j.jclepro.2018.11.175

Qin, H., Cheng, H., Li, H., and Wang, Y. (2020). Degradation of Ofloxacin, Amoxicillin and Tetracycline Antibiotics Using Magnetic Core-Shell MnFe2O4@C-NH2 as a Heterogeneous Fenton Catalyst. *Chem. Eng. J.* 396, 125304. doi:10.1016/j.cej.2020.125304

Rao, W., Lv, G., Wang, D., and Liao, L. (2018). Enhanced Degradation of Rh 6G by Zero Valent Iron Loaded on Two Typical Clay Minerals with Different Structures under Microwave Irradiation. *Front. Chem.* 6, 463. doi:10.3389/fchem.2018.00463

Suazo-Hernández, J., Sepúlveda, P., Manquián-Cerda, K., Ramírez-Tagle, R., Rubio, M. A., Bolan, N., et al. (2019). Synthesis and Characterization of Zeolite-Based Composites Functionalized with Nanoscale Zero-Valent Iron for Removing Arsenic in the Presence of Selenium from Water. *J. Hazard. Mater.* 373, 810–819. doi:10.1016/j.jhazmat.2019.03.125

Sun, J., Cui, L., Gao, Y., He, Y., Liu, H., and Huang, Z. (2021). Environmental Application of Magnetic Cellulose Derived from Pennisetum Sinese Roxb for Efficient Tetracycline Removal. *Carbohydr. Polym.* 251, 117004. doi:10.1016/j.carbpol.2020.117004

Sun, Z., Huang, D., Duan, X., Hong, W., and Liang, J. (2020). Functionalized Nanoflower-like Hydroxyl Magnesium Silicate for Effective Adsorption of Aflatoxin B1. *J. Hazard. Mater.* 387, 121792. doi:10.1016/j.jhazmat.2019.121792

Thao, N. T., Nhu, N. T., and Lin, K.-S. (2018). Liquid Phase Oxidation of Benzyl Alcohol to Benzaldehyde over Sepiolite Loaded Chromium Oxide Catalysts. *J. Taiwan Inst. Chem. Eng.* 83, 10–22. doi:10.1016/j.jtice.2017.11.034

Wang, C., Sun, R., Huang, R., and Wang, H. (2021). Superior fenton-like Degradation of Tetracycline by Iron Loaded Graphitic Carbon Derived from Microplastics: Synthesis, Catalytic Performance, and Mechanism. *Sep. Purif. Tech.* 270, 118773. doi:10.1016/j.seppur.2021.118773

Wang, X., Wang, A., Ma, J., and Fu, M. (2017). Facile green Synthesis of Functional Nanoscale Zero-Valent Iron and Studies of its Activity toward Ultrasound-Enhanced Decolorization of Cationic Dyes. *Chemosphere* 166, 80–88. doi:10.1016/j.chemosphere.2016.09.056

Wang, X., Zhang, B., Ma, J., and Ning, P. (2020). Novel Synthesis of Aluminum Hydroxide Gel-Coated Nano Zero-Valent Iron and Studies of its Activity in Flocculation-Enhanced Removal of Tetracycline. *J. Environ. Sci.* 89, 194–205. doi:10.1016/j.jes.2019.09.017

Wu, Q., Yang, H., Kang, L., Gao, Z., and Ren, F. (2020). Fe-based Metal-Organic Frameworks as Fenton-like Catalysts for Highly Efficient Degradation of Tetracycline Hydrochloride over a Wide pH Range: Acceleration of Fe(II)/Fe(III) Cycle under Visible Light Irradiation. *Appl. Catal. B: Environ.* 263, 118282. doi:10.1016/j.apcatb.2019.118282

Wu, S., Duan, Z., Hao, F., Xiong, S., Xiong, W., Lv, Y., et al. (2017). Preparation of Acid-Activated sepiolite/Rhodamine B@SiO2 Hybrid Fluorescent Pigments with High Stability. *Dyes Pigm.* 137, 395–402. doi:10.1016/j.dyepig.2016.10.030

Xin, S., Liu, G., Ma, X., Gong, J., Ma, B., Yan, Q., et al. (2021). High Efficiency Heterogeneous Fenton-like Catalyst Biochar Modified CuFeO2 for the Degradation of Tetracycline: Economical Synthesis, Catalytic Performance and Mechanism. *Appl. Catal. B: Environ.* 280, 119386. doi:10.1016/j.apcatb.2020.119386

Xu, D., Gao, Y., Lin, Z., Gao, W., Zhang, H., Karnowo, K., et al. (2020). Application of Biochar Derived from Pyrolysis of Waste Fiberboard on Tetracycline Adsorption in Aqueous Solution. *Front. Chem.* 7, 943. doi:10.3389/fchem.2019.00943

Yang, Y., Zhang, X., Chen, Q., Li, S., Chai, H., and Huang, Y. (2018). Ultrasound-Assisted Removal of Tetracycline by a Fe/N-C Hybrids/H2O2 Fenton-like System. *Acs Omega* 3, 15870–15878. doi:10.1021/acsomega.8b02581

Yazdani, M., Ebrahimi-Nik, M., Heidari, A., and Abbaspour-Fard, M. H. (2019). Improvement of Biogas Production from Slaughterhouse Wastewater Using Biosynthesized Iron Nanoparticles from Water Treatment Sludge. *Renew. Energ.* 135, 496–501. doi:10.1016/j.renene.2018.12.019

Zhang, H., Zhou, L., Li, J., Rong, S., Jiang, J., and Liu, S. (2021). Photocatalytic Degradation of Tetracycline by a Novel (CMC)/MIL-101(Fe)/β-CDP Composite Hydrogel. *Front. Chem.* 8, 593730. doi:10.3389/fchem.2020.593730

Zhang, N., Chen, J., Fang, Z., and Tsang, E. P. (2019). Ceria Accelerated Nanoscale Zerovalent Iron Assisted Heterogenous Fenton Oxidation of Tetracycline. *Chem. Eng. J.* 369, 588–599. doi:10.1016/j.cej.2019.03.112

Zhang, Y., Jiao, X., Liu, N., Lv, J., and Yang, Y. (2020). Enhanced Removal of Aqueous Cr(VI) by a green Synthesized Nanoscale Zero-Valent Iron Supported on Oak wood Biochar. *Chemosphere* 245, 125542. doi:10.1016/j.chemosphere.2019.125542

Zhang, Y., Shi, J., Xu, Z., Chen, Y., and Song, D. (2018). Degradation of Tetracycline in a schorl/H2O2 System: Proposed Mechanism and Intermediates. *Chemosphere* 202, 661–668. doi:10.1016/j.chemosphere.2018.03.116

Zhao, Z., Zhang, G., Zhang, Y., Dou, M., and Li, Y. (2020). Fe3O4 Accelerates Tetracycline Degradation during Anaerobic Digestion: Synergistic Role of Adsorption and Microbial Metabolism. *Water Res.* 185, 116225. doi:10.1016/j.watres.2020.116225

Zhou, Y., Wang, T., Zhi, D., Guo, B., Zhou, Y., Nie, J., et al. (2019). Applications of Nanoscale Zero-Valent Iron and its Composites to the Removal of Antibiotics: a Review. *J. Mater. Sci.* 54, 12171–12188. doi:10.1007/s10853-019-03606-5

Conflict of Interest: The authors declare that the research was conducted in the absence of any commercial or financial relationships that could be construed as a potential conflict of interest.

Publisher's Note: All claims expressed in this article are solely those of the authors and do not necessarily represent those of their affiliated organizations, or those of the publisher, the editors and the reviewers. Any product that may be evaluated in this article, or claim that may be made by its manufacturer, is not guaranteed or endorsed by the publisher.